NASA TN D-179

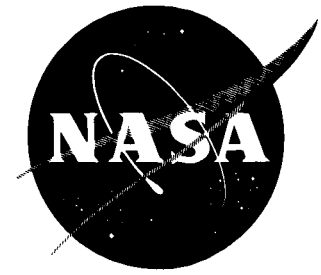

TECHNICAL NOTE

D-179

MEASUREMENTS OF PRESSURE AND LOCAL HEAT TRANSFER ON A 20° CONE AT ANGLES OF ATTACK UP TO 20° FOR A MACH NUMBER OF 4.95

By Jerome D. Julius

Langley Research Center
Langley Field, Va.

NATIONAL AERONAUTICS AND SPACE ADMINISTRATION

WASHINGTON December 1959

NATIONAL AERONAUTICS AND SPACE ADMINISTRATION

TECHNICAL NOTE D-179

MEASUREMENTS OF PRESSURE AND LOCAL HEAT TRANSFER ON A 20° CONE AT ANGLES OF ATTACK UP TO 20° FOR A MACH NUMBER OF 4.95

By Jerome D. Julius

SUMMARY

The distribution of pressure and local heat transfer on a 20° included-angle cone at a Mach number of 4.95 and at angles of attack up to 20° were measured. Data were obtained in a Reynolds number range of 14×10^6 to 75×10^6 per foot based on free-stream conditions.

The measured pressures were compared with the first-order and second-order approximations of exact cone theory and with Newtonian and modified Newtonian theory. The data were best predicted by Newtonian theory.

The heat-transfer rates along the most windward generator of the cone increased with increasing angle of attack. The theories of NACA Technical Notes 4152, 4380, and 4208 were compared with the present data. They provided reasonable predictions of the experimental data when the pressure was determined to the second order (Tech. Rep. No. 5, M.I.T. cone tables) and other local conditions were determined to the first order (Tech. Rep. No. 3, M.I.T., cone tables). Heat transfer was greatest along the most windward generator, $\phi = 0°$, when the flow was wholly laminar. When transition was observed, the $\phi = 30°$ generator generally showed the highest heat transfer.

INTRODUCTION

Although numerous investigations have presented experimental data and theoretical analyses concerning the heat-transfer rates for a cone at zero angle of attack, only a comparatively small amount of work has been done for a cone at other angles of attack. (For one such experimental investigation, see ref. 1.) Certain theoretical considerations (refs. 2, 3, and 4) have been proposed by which the laminar and turbulent heat-transfer rates may be estimated for the most windward generator (Peripheral angle = 0°) of a cone at angle of attack.

In reference 2, the equations of the compressible laminar boundary layer for the most windward streamline of a yawed cone were presented, and solutions were obtained for a Prandtl number equal to 1 for both insulated and cooled surfaces. A calculation was also provided to show the effect on heat-transfer coefficient of a Prandtl number less than 1.

In reference 3, through the use of integral techniques, approximate solutions to the compressible-laminar-boundary-layer equations along the most windward streamline of a cone were obtained. By using the Chapman-Rubesin temperature-viscosity relation and a Prandtl number of 1, the Stanton number may be computed.

In reference 4, momentum integral equations were derived for the compressible turbulent boundary layer on an arbitrary curved surface. Solutions suitable for the computation of the local skin-friction coefficient on a cone at angle of attack were presented, and the Stanton number was obtained through the use of Reynolds analogy.

Each of the above analyses depends upon obtaining the local stream conditions on the cone just outside the boundary layer, as given in the M.I.T. cone tables (refs. 5, 6, and 7). The exception to this is the section of reference 2 entitled "Very Large Angle of Attack" in which analogy is made to a yawed infinite cylinder. Obtaining local stream conditions with the use of these tables is not always simple due to the brevity of the tables. The problem thus arises as to the precision with which the local conditions must be computed to obtain sufficient accuracy of the heat-transfer prediction from the various theoretical methods, and furthermore, which of the theories gives the best estimates for a given order of precision.

This paper presents the results of an experimental investigation of the pressure distribution and heat-transfer rates to a 20° included-angle cone at angles of attack of 0°, 10°, and 20° and compares the results with the theories described herein.

SYMBOLS

A_{av} average skin area, equal to reference volume divided by skin thickness

A_w external skin reference area

c_p specific heat of air at constant pressure, Btu/(slug)($^\circ$R)

c_w heat capacity of wall material, Btu/(lb)($^\circ$R)

h	local heat-transfer coefficient, Btu/(sec)(sq ft)(^{o}R)
h_m	measured (uncorrected) heat-transfer coefficient, Btu/(sec)(sq ft)(^{o}R)
m	reference mass of skin, lb
N_{St}	Stanton number, $\frac{h}{\rho c_p V}$
p	pressure, lb/sq ft
Q	quantity of heat transferred per unit time, Btu/sec
R	unit Reynolds number $\frac{\rho V}{\mu}$, $\frac{1}{ft}$
R_x	local Reynolds number based on conditions external to the boundary layer and distance along the cone surface from the apex, $\frac{\rho_l V_l x}{\mu_l}$
T	temperature, ^{o}R
T_r	recovery (or adiabatic wall) temperature, ^{o}R
t	time, sec
V	flow velocity, ft/sec
x	surface distance measured from apex
α	angle of attack
β	cone half-angle
μ	viscosity, slugs/ft-sec
ρ	density of air, slugs/cu ft
ϕ	peripheral angle (measured from the windward generator)
τ_w	skin thickness, ft

Subscripts:

l	local conditions external to boundary layer
w	wall or skin values
∞	undisturbed free-stream conditions
ϕ	peripheral angle

APPARATUS AND PROCEDURE

Tunnel

The tests were conducted in a 9-inch-diameter blowdown axisymmetric jet in the Langley gas dynamics laboratory. The test-section Mach number was 4.95. All tests were conducted at a stagnation temperature of approximately 860° R. The stagnation pressure was varied to provide a range of Reynolds numbers per foot from 14×10^6 to 75×10^6.

Models

A sketch of the model configuration is shown in figure 1. The models were constructed of 17-4 PH stainless steel. The skin thickness was nominally 0.060 inch, but for more accurate determination of the skin thickness, the heat-transfer model was cut open at the completion of the tests to facilitate measurement with a micrometer. The micrometer readings were then used as the local skin thickness in reducing the heat-transfer data. The nose radius of the model was about 0.005 inch.

One heat-transfer and one pressure model were constructed. The pressure model was polished to about 15 microinches, and the heat-transfer model was polished until the average roughness was not greater than 2 microinches as measured on an interference microscope. The pressure model had a single row of orifices along one generator of the cone, and the heat-transfer model had a row of thermocouples spot-welded to the inner surface of the skin. The surface distance from the apex at which each of the orifices and thermocouples was located is indicated in figure 1. The peripheral distributions of pressure and heat-transfer rate around the cones were obtained by rotating the cones on their axes between tests.

Test Conditions

Pressure model.- The static pressure along the cone surface was measured at angles of attack of 0°, 10°, and 20° at a free-stream Mach number of 4.95. At an angle of attack of 0°, the static pressure was measured for a range of Reynolds number per foot of 15×10^6 to 75×10^6 at $\phi = 180^\circ$ and at $\phi = 0^\circ$ for a Reynolds number per foot of 30×10^6. At angles of attack of 10° and 20° measurements were made at peripheral angles of 0°, 30°, 60°, 90°, and 180°, at a Reynolds number per foot of 30×10^6. All measurements were made on a mercury manometer.

Heat-transfer model.- The heat-transfer model was tested at a free-stream Mach number of 4.95, for a range of Reynolds numbers per foot of 14×10^6 to 70×10^6 at angles of attack of 0°, 10°, and 20°. For angles of attack of 10° and 20°, the model was tested at peripheral angles of 0°, 30°, 60°, 90°, and 180°. Additional tests were conducted with the heat-transfer model after it had been roughened near the apex. The apex of the model was covered with 0.005-inch carborundum grains bonded with a phenolic cement for a length of approximately 0.25 inch. (See fig. 2.)

For the heat-transfer test, the tunnel was started and brought to steady operating conditions with the model outside the tunnel. Then, a vertical panel which covered the test-section opening was lowered, and the model, which was mounted on the test-section door, was injected into the test section by a pneumatic actuator. It has been determined in another test that the time from the instant the model first begins to move into the airstream until it reaches its rest position and steady flow is reestablished is approximately 0.05 second.

The model remained in the airstream from 3 to 5 seconds, and then it was retracted. It was cooled to approximately room temperature before the succeeding run. The data were recorded on an 18-channel recording oscillograph and evaluated at the instant the model had been in the airstream for 0.5 second.

Further tests were conducted at zero angle of attack only in order to obtain experimental recovery factors. For these tests, the model remained in the airstream for approximately 3 minutes, and the data were evaluated at 2.5 minutes. Very little change in the thermocouple readings occurred after about 30 seconds. A small change could be observed in the vicinity of transition, which could be attributed to longitudinal-conduction effects.

Data Reduction

The measured heat-transfer coefficient is obtained from the temperature-time data by using the heat-balance equation

$$h_m(T_r - T_w) = \frac{mc_w}{A_w}\frac{dT}{dt}$$

The experimental data were corrected to account for the finite conductivity in the direction normal to the cone surface. This correction, which is discussed in more detail in reference 8, can be approximated by

$$\frac{h}{h_m} = 1 + 0.65h_m$$

for the particular model and conditions of these tests. No correction was made for lateral conduction. However, since the data were reduced at 0.5 second after immersing the model in the flow, the model temperature was not changed greatly from its initial isothermal state, so that lateral conduction does not affect the accuracy of most of the data. One possible exception is pointed out in the Results and Discussion section.

Correction to the data was also made to account for the fact that for a cone of finite skin thickness the external area of the skin is greater than the mean area. The correction is of the form

$$\frac{A_{av}}{A_w} = 1 - \frac{\tau_w}{2x \tan \beta}$$

where A_{av} is the average area of a reference segment of the skin having external area A_w.

The laminar and turbulent recovery factors determined experimentally at zero angle of attack were 0.872 and 0.915, respectively, which correspond approximately to the square root and cube root of the Prandtl number based on local stream temperature. In reducing the data for angle of attack other than zero, the adiabatic wall temperature was calculated by assuming that the same recovery factors held. This is equivalent to neglecting a variation of recovery factor with temperature for the range of local static temperatures encountered in this experiment.

Determination of Local Conditions and Certain Heat-Transfer Parameters

It is necessary to evaluate the local conditions on the yawed cone to reduce the experimental data or to work numerical examples of the theories of references 2 and 3. The local conditions, as well as certain other necessary heat-transfer parameters, were computed from references 5, 6, 7, and 9, in which each quantity is expressed as a power series in α.

As a first approximation, only first-order terms (ref. 6) were computed for all quantities. This method is referred to hereinafter as "method 1." However, as will be shown, the first-order prediction of pressure on the yawed cone shows poor agreement with the experimental data, particularly at $\alpha = 20^{\circ}$. Also, the laminar-boundary-layer heat transfer on the windward streamline was not accurately predicted by the theories when conditions were determined by this first-order method. Therefore, the pressure expression was recomputed to include second-order terms (ref. 7). The local conditions were then given to second order for pressure but to first order for all others. This method is referred to as "method 2."

The integrals of reference 4 were evaluated by using the techniques of appendix D in reference 10.

RESULTS AND DISCUSSION

Pressure Distribution

The experimental pressure distribution along the cone surface for zero angle of attack is presented in figure 3. The data were compared with the results of reference 5. The comparison is favorable for the forward portion of the cone. The decreasing pressure near the rear of the model was a tunnel effect which has appeared consistently on other models as well for this tunnel station. It can be noted that for zero angle of attack, unit Reynolds number and peripheral rotation of the orifices have only slight effects on the pressure distribution.

The peripheral pressure distributions for several axial stations on the cone at angles of attack are shown in figure 4. The data are compared with references 5, 6, 7, and 11. Both the first-order and second-order approximation of references 5, 6, and 7 are shown, along with Newtonian theory and modified Newtonian theory of reference 11, without centrifugal-force corrections. Newtonian theory was modified by using the proper stagnation-point fluid properties behind a normal

shock for a Mach number of 4.95. The pressure disturbance at the rear of the model, noted at zero angle of attack, was apparent at other angles of attack beyond the station at $x = 4.25$ inches. Therefore, the pressure data for $x > 4.00$ inches have not been included.

At an angle of attack of 10°, the first-order approximation was not as good as the second-order approximation or the Newtonian and modified Newtonian theories.

At an angle of attack of 20°, the Newtonian theory was the best approximation of the data. For $\phi = 0^\circ$ to $\phi = 30^\circ$, both the second-order approximation and the Newtonian theory were good estimates of the data, but at $\phi = 100^\circ$ the second-order approximation becomes negative, and it therefore appears unsuitable except in the vicinity of $\phi = 0^\circ$.

For comparison, the calculated pressure on the stagnation line of a yawed infinite cylinder is shown on figure 4(b). The cylinder was assumed to be yawed 60° to the normal, thus making its stagnation line parallel to the most windward generator of the cone at $\alpha = 20^\circ$. If the cylinder was assumed to be yawed 70°, making its axis parallel to that of the cone, the calculated pressure would, of course, have been lower.

Heat Transfer Along the Most Windward Generator

Angle of attack of 0°.- The experimental heat-transfer data for an angle of attack of 0° for $\phi = 0^\circ$ are shown in figure 5 in which local Stanton number N_{St} is plotted against local Reynolds number R_x. The laminar-boundary-layer data are compared with the theories of references 2 and 12; the turbulent-boundary-layer data are compared (assuming completely turbulent flow from the nose) with the theories of references 4 and 12. For the laminar-heat-transfer data the two theories predict the value of the data equally well within the scatter of the data. The Stanton numbers of the turbulent heating rates are better predicted by the theory of reference 4, that of reference 12 being approximately 15 per cent higher.

Angle of attack of 10°.- The experimental heat-transfer data for an angle of attack of 10° for $\phi = 0^\circ$ are shown in figure 6. The data are compared with the theories of references 2 to 4. In figure 6(a), method 1 was used to compute the local conditions, and in figure 6(b) method 2 was used. The theory remains the same in either case. For the laminar boundary layer, the predictions of references 2 and 3 agree within 2 percent. The theories of references 2 and 3 predict the Stanton number for the laminar case fairly well for method 2, but are somewhat low for method 1. The laminar experimental data for an angle

of attack of 10° were approximately 45 percent higher than the laminar data at an angle of attack of 0°.

The theory of reference 4 gives a good estimation of the turbulent-boundary-layer data which were scattered. The experimental turbulent-boundary-layer data at $\alpha = 10^\circ$ were approximately 25 percent higher than that at an angle of attack of 0°.

20° angle of attack.- The experimental heat-transfer data for 20° angle of attack for $\phi = 0^\circ$ are shown in figure 7. Again the theories of references 2 to 4 are compared with the data. In figure 7(a), the first method of computing the local conditions was used, and in figure 7(b) the second method was used. The theory remains the same in either case. For the laminar boundary layer, the theory of reference 3 provided a closer estimation of the data than that of reference 2. In the case of reference 2, the section entitled "Very Large Angle of Attack" was used along with some of the results of reference 13. In that section, a cone at large angle of attack (angles greater than or equal to the cone included angle) was treated as a yawed infinite cylinder. In computing the theory of reference 2 shown in figure 7, the cylinder yaw was assumed to be 70°, which made its axis parallel to the cone axis. However, since the pressure on the stagnation line of the cylinder would be low compared to that on the cone at $\alpha = 20^\circ$ (fig. 4(b)), the experimental value of the cone pressure has been used. The poorer agreement of reference 2 with the data was probably due to the difference between the local conditions on a truly yawed infinite cylinder and a cone. The laminar-boundary-layer data at an angle of attack of 20° were approximately 75 percent higher than that at an angle of attack of 0°.

The theory of reference 4 gives a prediction which is slightly above the average magnitude of the turbulent-boundary-layer data. The experimental turbulent-boundary-layer data for an angle of attack of 20° were approximately 60 percent higher than that at an angle of attack of 0°.

The data for $\alpha = 20^\circ$ show a tendency to have less dependency of the Stanton number on Reynolds number than the theory predicts. It may be seen in figure 7(b) that the laminar data depart from the theoretical curve for low Reynolds numbers and that the turbulent data are nearly independent of x for a given test (constant Reynolds number per foot). This is possibly caused by the peripheral conduction of heat away from the most windward generator. Near the nose, where the radius is small, the lateral temperature gradient is most severe, and the conduction would be greater than on the rear portion of the model. As mentioned previously, no correction has been made to the data to account for lateral conduction.

Effects of Angle of Attack on Boundary-Layer Transition

Although boundary-layer transition was not under direct investigation, the data show a noteworthy trend. At an angle of attack of 0° (fig. 5), the Reynolds number of boundary-layer transition increases as the Reynolds number per foot increased. This trend has been noted on other models tested in this jet and is commonly observed in other wind tunnels as well. However, the data for angles of attack of 10° and 20° (figs. 6 and 7) show that on the most windward generator, the trend is reversed; that is, the transition Reynolds number decreases with increasing Reynolds number per foot. No satisfactory explanation for this reversal presents itself.

Turbulent heating rates for an artifically induced turbulent boundary layer.- The heat-transfer rates were measured for $\phi = 0^\circ$. The experimental data are shown in figures 8(a), 8(b), and 8(c) for angles of attack of 0°, 10°, and 20°, respectively. The magnitude of the experimental data for the artificially induced turbulent boundary layer and that produced by natural transition were the same. Only the results, when the local conditions were computed using method 2, are shown. At $\alpha = 20^\circ$, the data show considerable scatter, at least part of which may be attributed to the lateral-conduction effects mentioned previously.

Heat-transfer distribution around the cone.- The local experimental heat-transfer coefficient h was divided by the theoretical laminar heat-transfer coefficient at $\phi = 0^\circ$ and plotted against peripheral angle ϕ, for angles of attack of 10° and 20°. The results are shown in figure 9. The theoretical laminar heat-transfer coefficient was determined from the results of reference 3. In computing the experimental heat-transfer coefficient for various values of ϕ, the adiabatic wall temperature was held constant at the value computed for a laminar boundary layer on the stagnation streamline. This avoids introducing a somewhat arbitrary static temperature distribution into the computation, but allows for small differences in stagnation temperature for the different tests and in wall temperatures. Figure 9(a) shows that laminar-boundary-layer flow existed for all values of ϕ only when the unit Reynolds number was 14×10^6 per foot at an axial location of 1.00 inch. Figure 9(b) shows that laminar-boundary-layer flow existed for all values of ϕ when the unit Reynolds number was 14×10^6 per foot at axial locations of 1.00 and 1.75 inches and also when the unit Reynolds number was 28×10^6 per foot at an axial location of 1.00 inch. All other positions on figures 9(a) and 9(b) experienced either transitional flow or turbulent-boundary-layer flow.

The position of maximum heat transfer was generally at $\phi = 30^\circ$ for these tests. It is believed that it was associated with the position of transition on the cone. Since the location of transition plays

such an important part in determining the distribution of heat-transfer rate around the periphery of the cone at angle of attack and since the location of transition cannot, in general, be predicted for other test conditions, only very limited conclusions may be drawn from the data of figure 9. The most important conclusion would appear to be that the highest heat-transfer rate occurs on the windward generator for those cases in which the flow is wholly laminar, but when transition is observed, the $\phi = 30^\circ$ generator generally showed the highest heat transfer.

SUMMARY OF RESULTS

An experimental investigation of the distributions of pressure and heat-transfer rate on a 20° included-angle cone has been made at angles of attack of 0°, 10°, and 20° at a Mach number of 4.95 for a range of Reynolds numbers per foot of 14×10^6 to 75×10^6 based on free-stream conditions. Pressure and heat transfer were measured for peripheral angles of 0° (windward generator), 30°, 60°, 90°, and 180°.

The pressure distribution was not predicted well by the results of the M.I.T. cone tables if only the first-order term of the power series was used, particularly at an angle of attack of 20°. However, inclusion of second-order terms greatly improved the prediction so that the agreement was good in the vicinity of the most windward generator. The Newtonian theory yielded better agreement with the experiment over the entire periphery of the cone.

On the windward generator, the heat transfer increased with increasing angle of attack. The maximum heat-transfer rate was measured on the most windward generator only when the flow was totally laminar. The most general position of maximum heat transfer was near $\phi = 30^\circ$ for tests in which transition was observed.

When the local conditions were determined by computing the pressure to second order and other quantities to first order, the agreement of the theories of NACA Technical Notes 4152, 4380, and 4208 with experiment was good. For the laminar data, the prediction of NACA Technical Note 4380 was better than that of NACA Technical Note 4152, particularly for an angle of attack of 20°.

Transition Reynolds number increased with increasing unit Reynolds number at an angle of attack of 0°, but on the windward generator, it

decreased with increasing unit Reynolds number at angles of attack of 10° and 20°.

Langley Research Center,
National Aeronautics and Space Administration,
Langley Field, Va., September 1, 1959.

REFERENCES

1. Sands, Norman, and Jack, John R.: Preliminary Heat-Transfer Studies on Two Bodies of Revolution at Angle of Attack at a Mach Number of 3.12. NACA TN 4378, 1958.

2. Reshotko, Eli: Laminar Boundary Layer with Heat Transfer on a Cone at Angle of Attack in a Supersonic Stream. NACA TN 4152, 1957.

3. Brunk, William E.: Approximate Method for Calculation of Laminar Boundary Layer with Heat Transfer on a Cone at Large Angles of Attack in Supersonic Flow. NACA TN 4380, 1958.

4. Braun, Willis H.: Turbulent Boundary Layer on a Yawed Cone in a Supersonic Stream. NACA TN 4208, 1958.

5. Staff of the Computing Section, Center of Analysis (Under Direction of Zdeněk Kopal): Tables of Supersonic Flow Around Cones. Tech. Rep. No. 1 (NOrd Contract No. 9169), M.I.T., 1947.

6. Staff of the Computing Section, Center of Analysis (Under Direction of Zdeněk Kopal): Tables of Supersonic Flow Around Yawing Cones. Tech. Rep. No. 3 (NOrd Contract No. 9169), M.I.T., 1947.

7. Staff of the Computing Section, Center of Analysis (Under Direction of Zdeněk Kopal): Tables of Supersonic Flow Around Cones of Large Yaw. Tech. Rep. No. 5 (NOrd Contract No. 8555 and 9169), M.I.T., 1949.

8. Trimpi, Robert L., and Jones, Robert A.: Transient Temperature Distribution in a Two-Component Semi-Infinite Composite Slab of Arbitrary Materials Subjected to Aerodynamic Heating With a Discontinous Change in Equilibrium Temperature or Heat-Transfer Coefficient. NACA TN 4308, 1958.

9. Young, G. B. W., and Siska, C. P.: Supersonic Flow Around Cones at Large Yaw, U.S. Air Force Project RAND, D-198, The RAND Corp., March 1, 1951.

10. Mirels, Harold: Boundary Layer Behind Shock or Thin Expansion Wave Moving Into Stationary Fluid. NACA TN 3712, 1956.

11. Grimminger, G., Williams, E. P., and Young, G. B. W.: Lift on Inclined Bodies of Revolution in Hypersonic Flow. Jour. Aero. Sci., vol. 17, no. 11, Nov. 1950, pp. 675-690.

12. Van Driest, E. R.: The Problem of Aerodynamic Heating. Aero. Eng. Rev., vol. 15, no. 10, Oct. 1956, pp. 26-41.

13. Reshotko, Eli, and Beckwith, Ivan E.: Compressible Laminar Boundary Layer Over a Yawed Infinite Cylinder With Heat Transfer and Arbitrary Prandtl Number. NACA Rep. 1379, 1958. (Supersedes NACA TN 3986.)

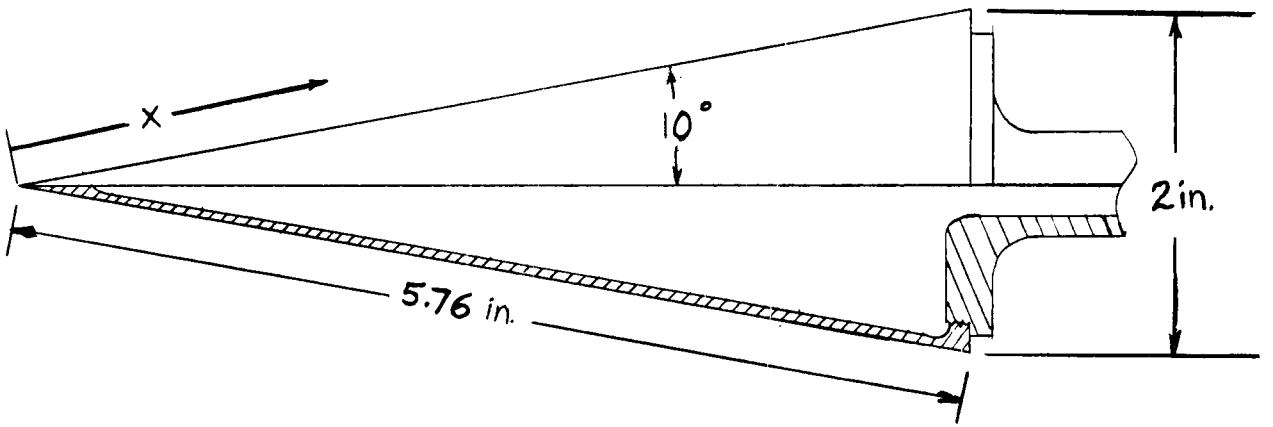

Thermocouple locations at surface distance, x, in.																	
1.00	1.25	1.50	1.75	2.00	2.25	2.50	2.75	3.00	3.25	3.50	3.75	4.00	4.25	4.50	4.75	5.00	5.25

Static pressure stations at surface distance, x, in.													
1.00	1.50	2.00	2.50	3.00	3.25	3.50	3.75	4.00	4.25	4.50	4.75	5.00	5.25

Figure 1.- Model geometry.

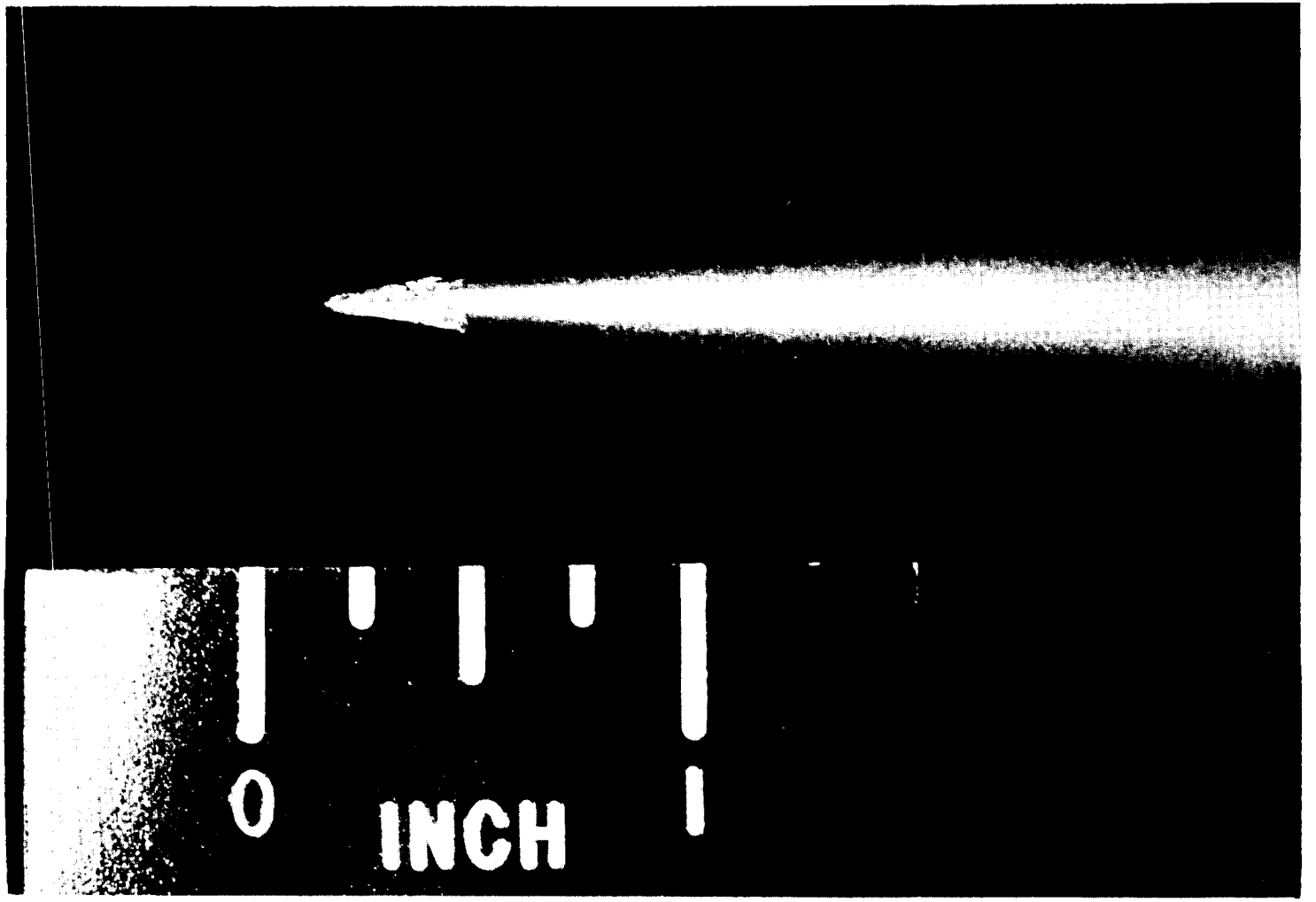

L-59-286

Figure 2.- Photograph of model tip with artificial roughness.

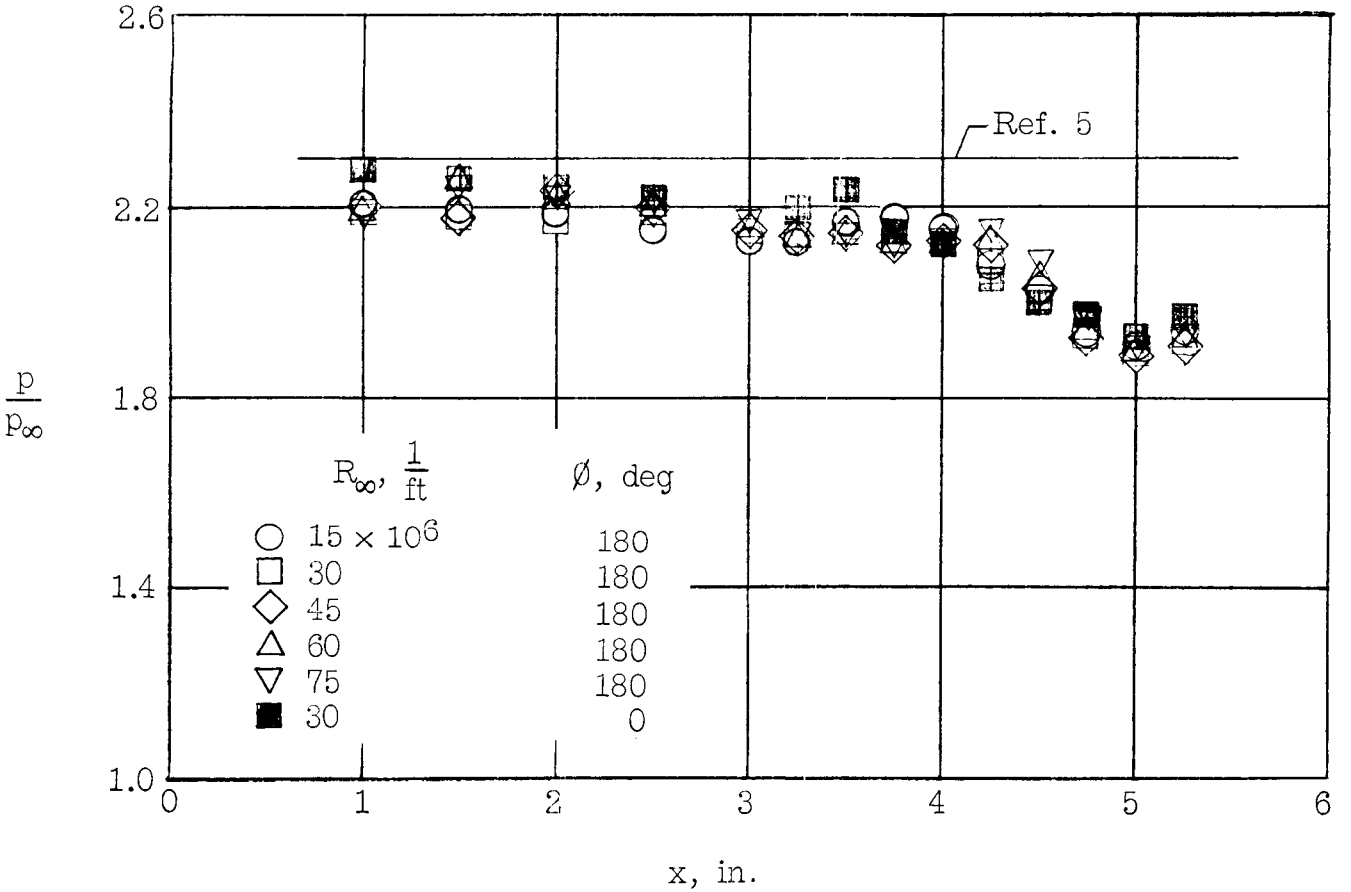

Figure 3.- Pressure distribution along the cone surface at $\alpha = 0^{\circ}$.

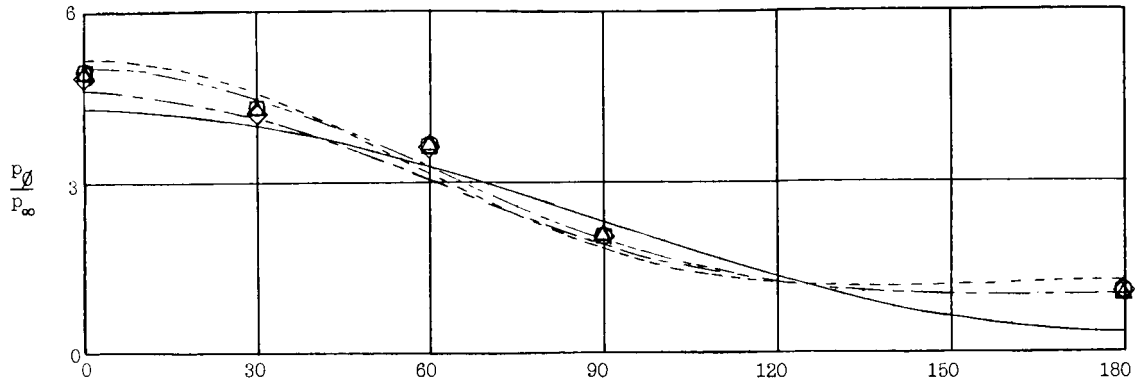

(a) $\alpha = 10^\circ$.

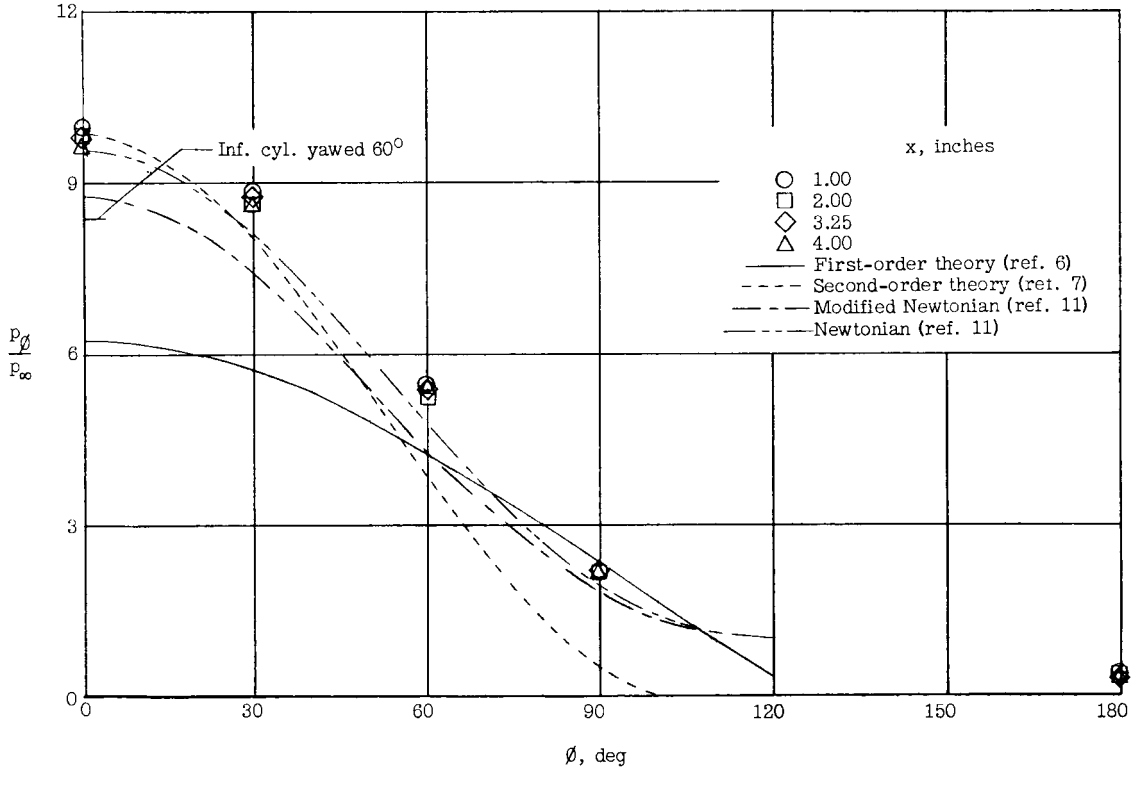

(b) $\alpha = 20^\circ$.

Figure 4.- Peripheral pressure distribution. $R_\infty = 30 \times 10^6 \frac{1}{ft}$.

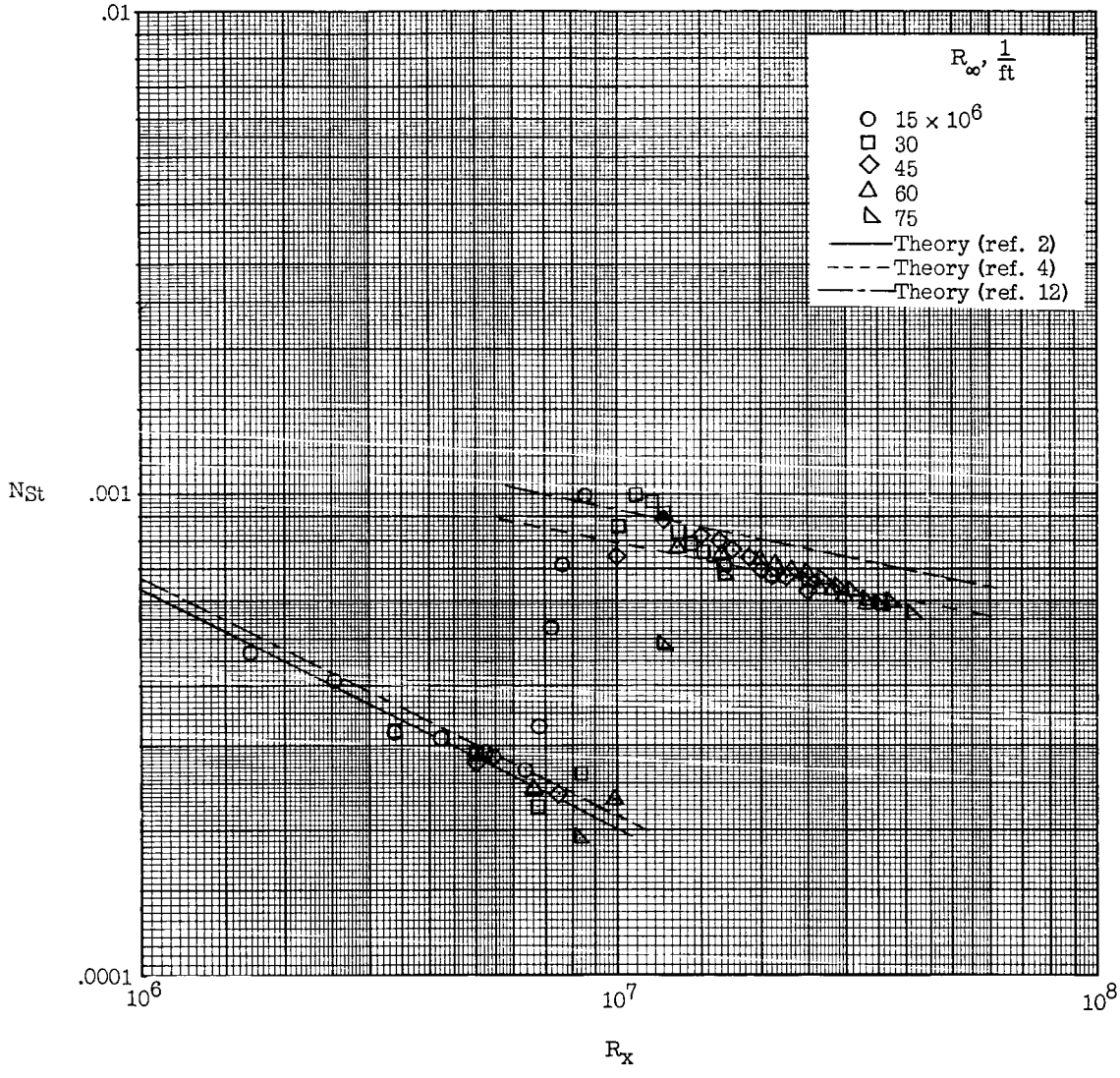

Figure 5.- Comparison of laminar- and turbulent-boundary-layer theories with experimental data for $\phi = 0^\circ$ and $\alpha = 0^\circ$.

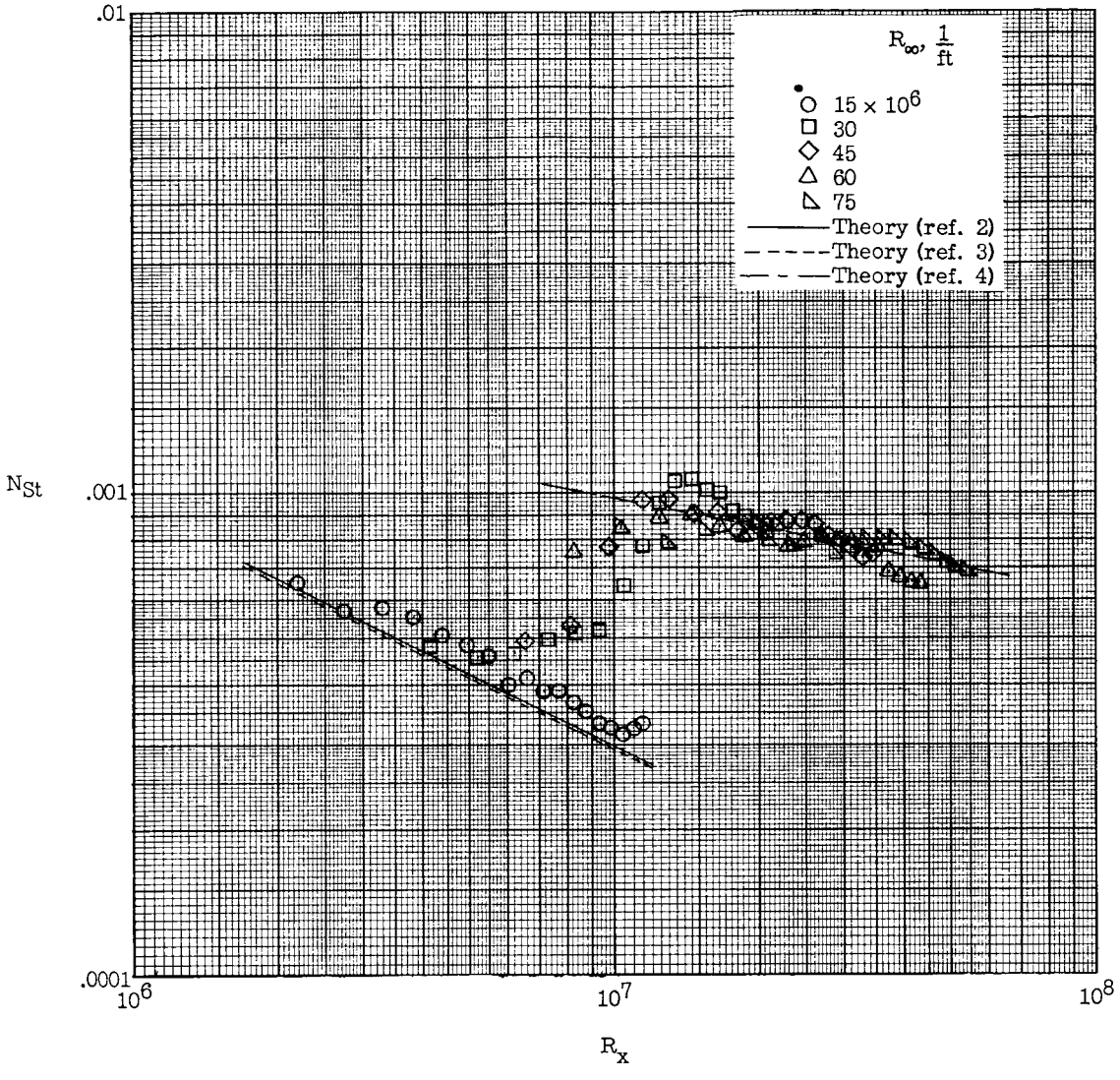

(a) Local conditions determined by method 1.

Figure 6.- Comparison of laminar- and turbulent-boundary-layer theories with experimental data for $\alpha = 10^\circ$ and $\phi = 0^\circ$.

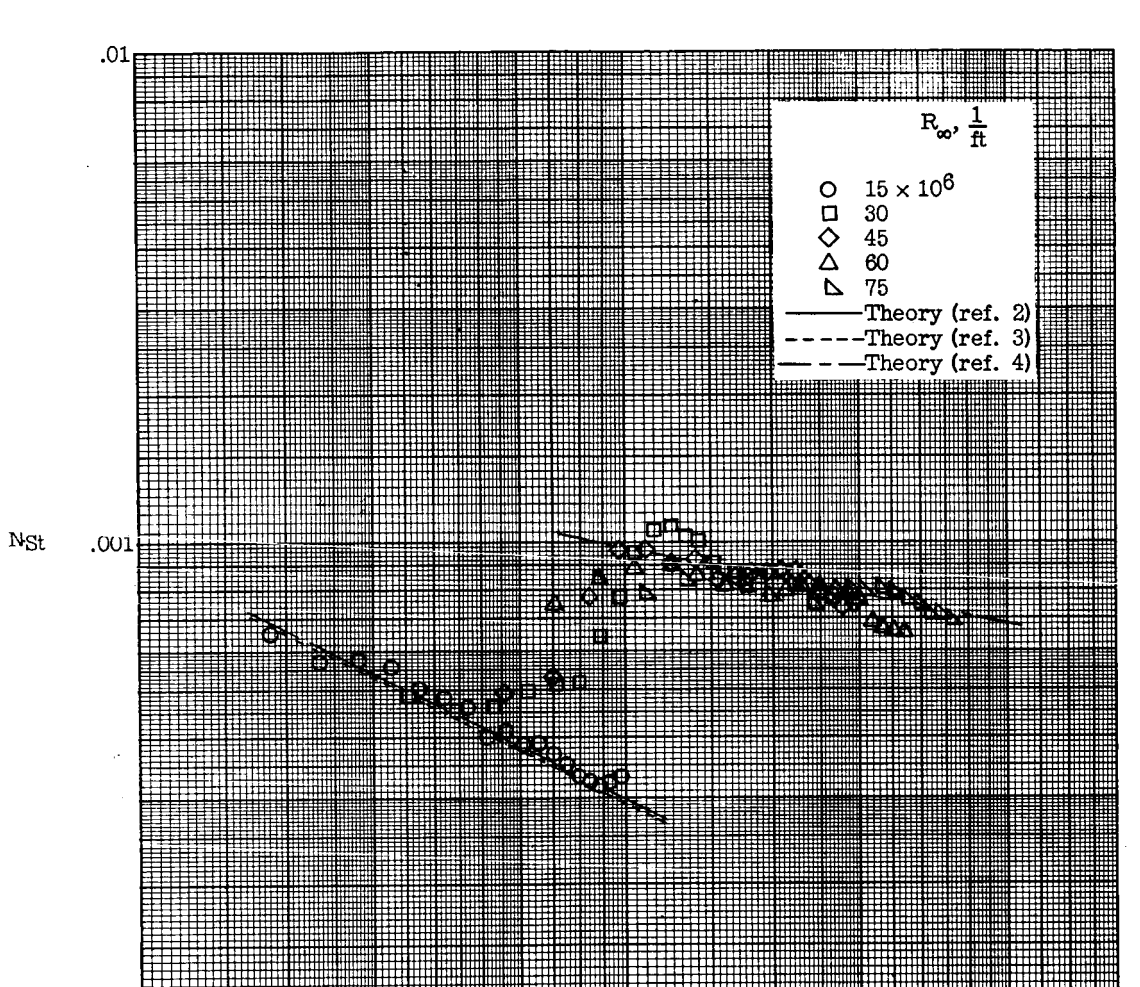

(b) Local conditions determined by method 2.

Figure 6.- Concluded.

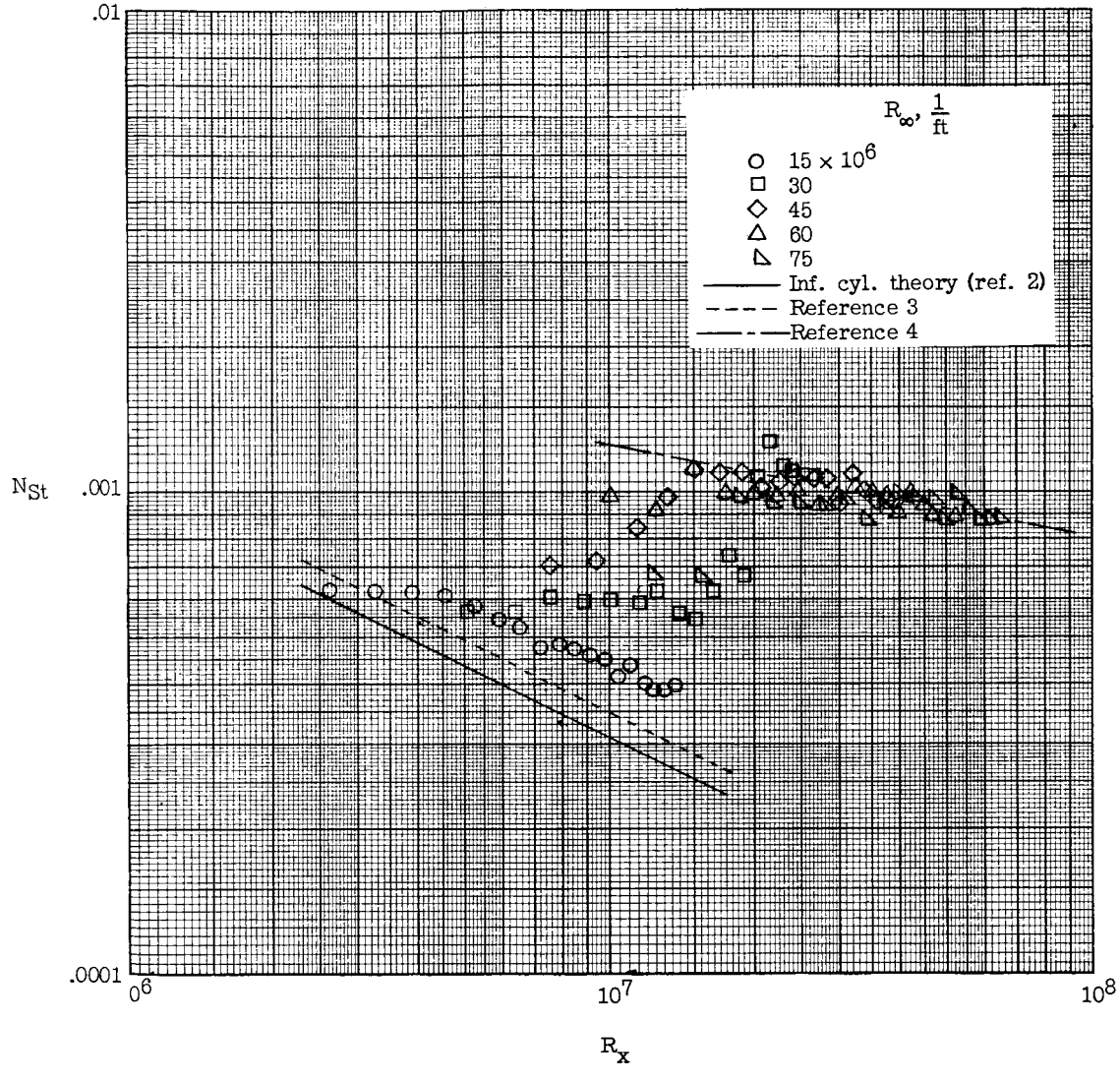

(a) Local conditions determined by method 1.

Figure 7.- Comparison of laminar- and turbulent-boundary-layer theories with experimental data for $\alpha = 20^\circ$ and $\phi = 0^\circ$.

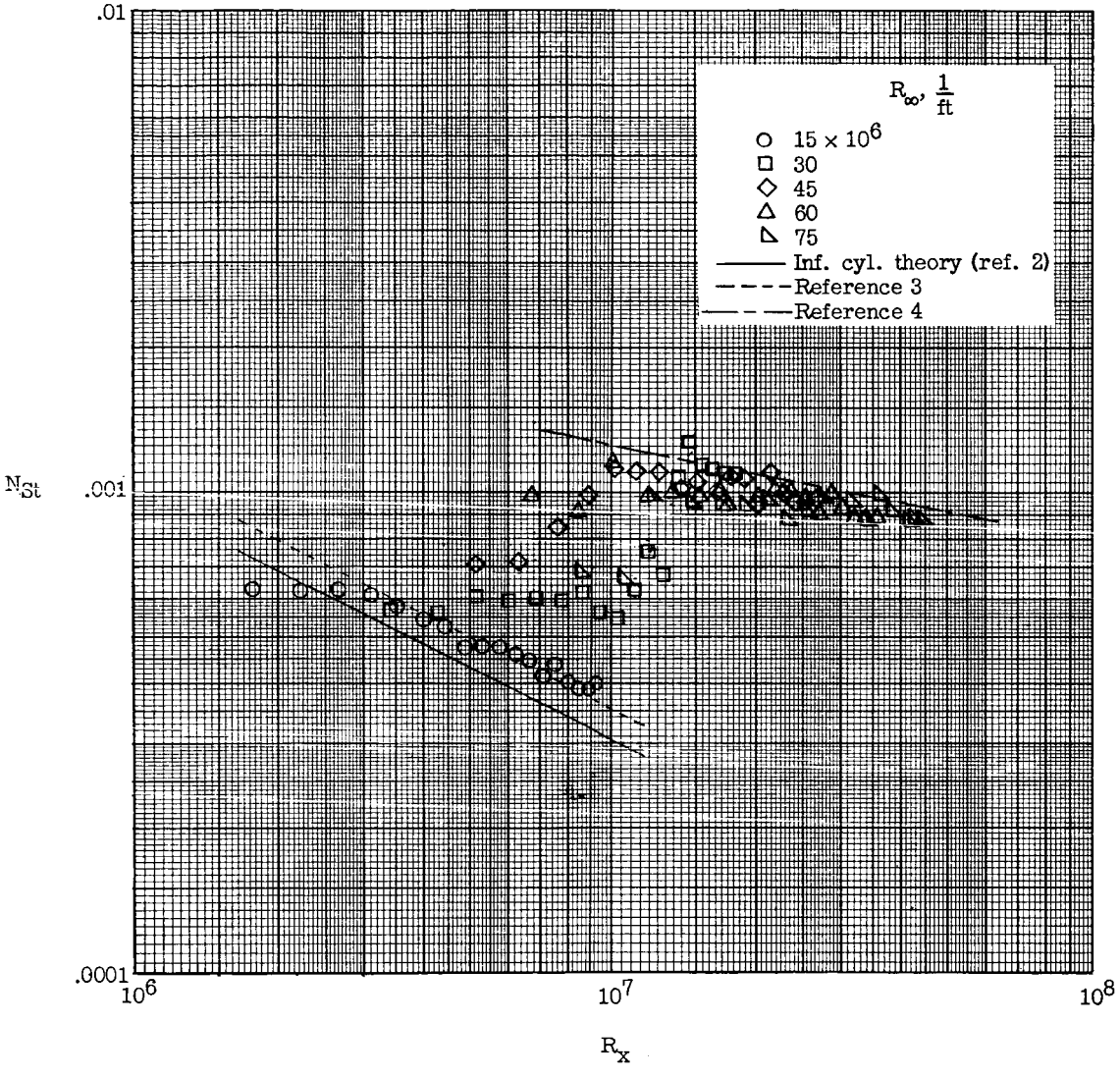

(b) Local conditions determined by method 2.

Figure 7.- Concluded.

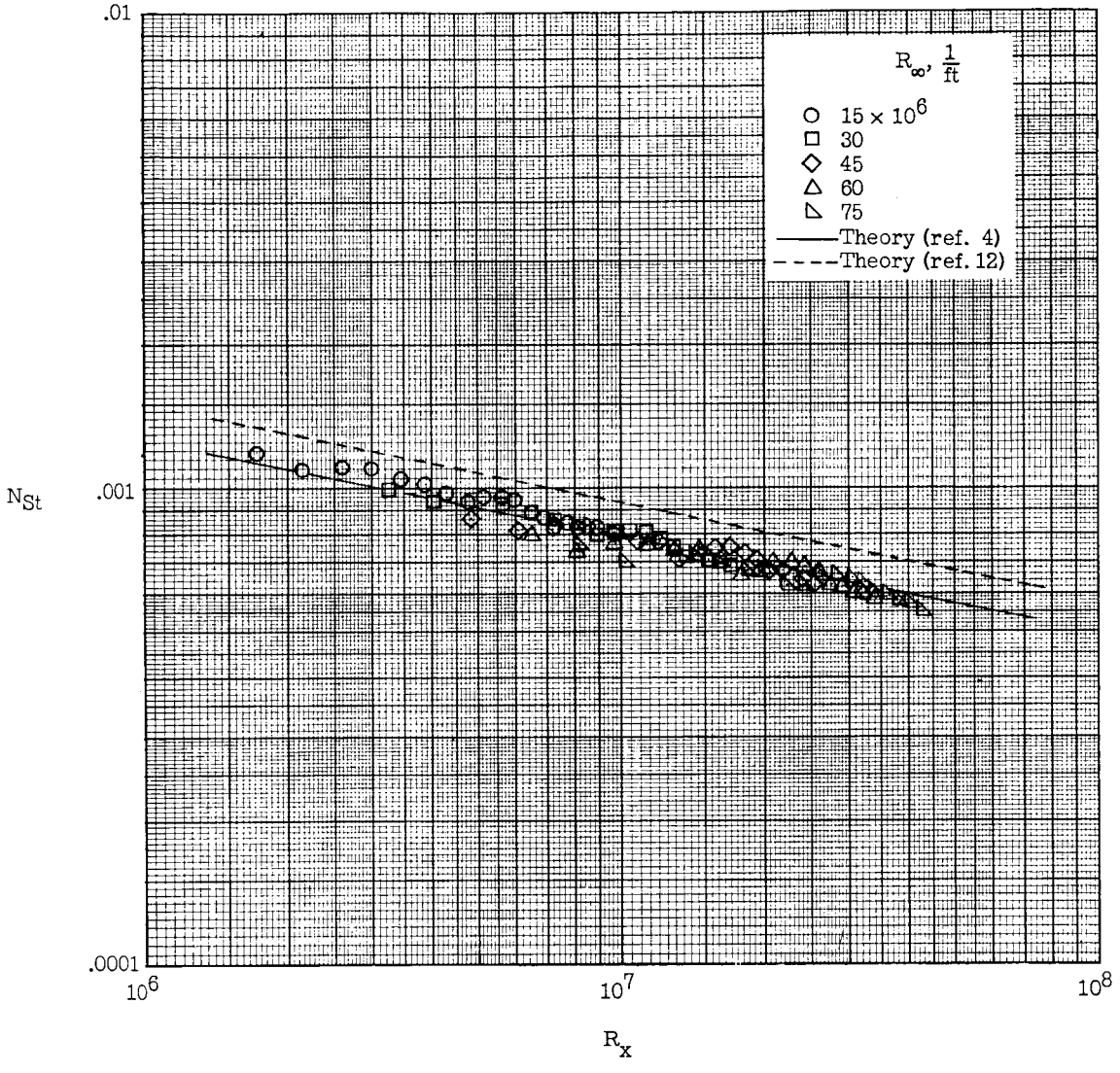

(a) $\alpha = 0^\circ$.

Figure 8.- Comparison of turbulent-boundary-layer theories with experimental data for $\phi = 0^\circ$. Computed by method 2.

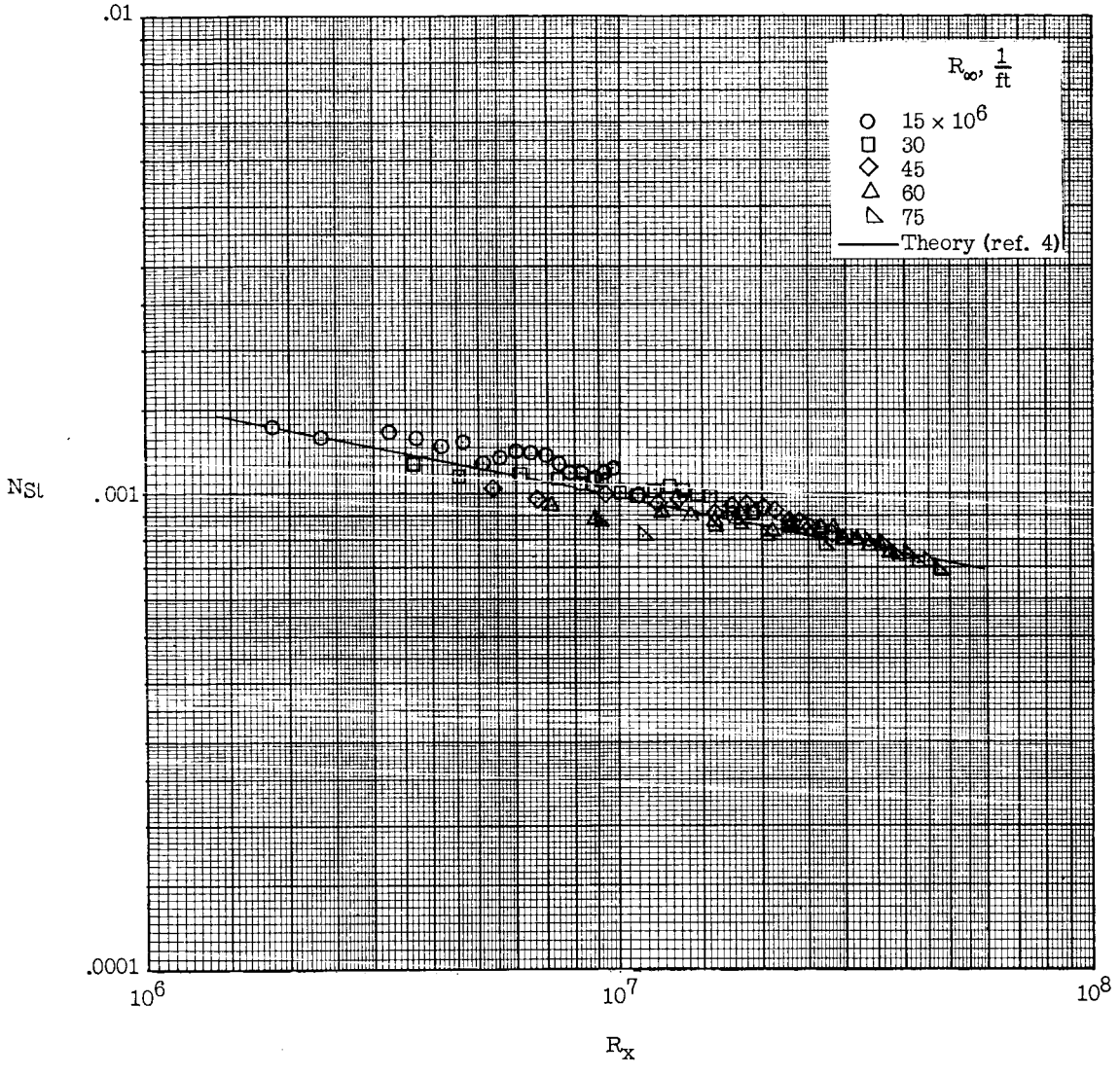

(b) $\alpha = 10^\circ$.

Figure 8.- Continued.

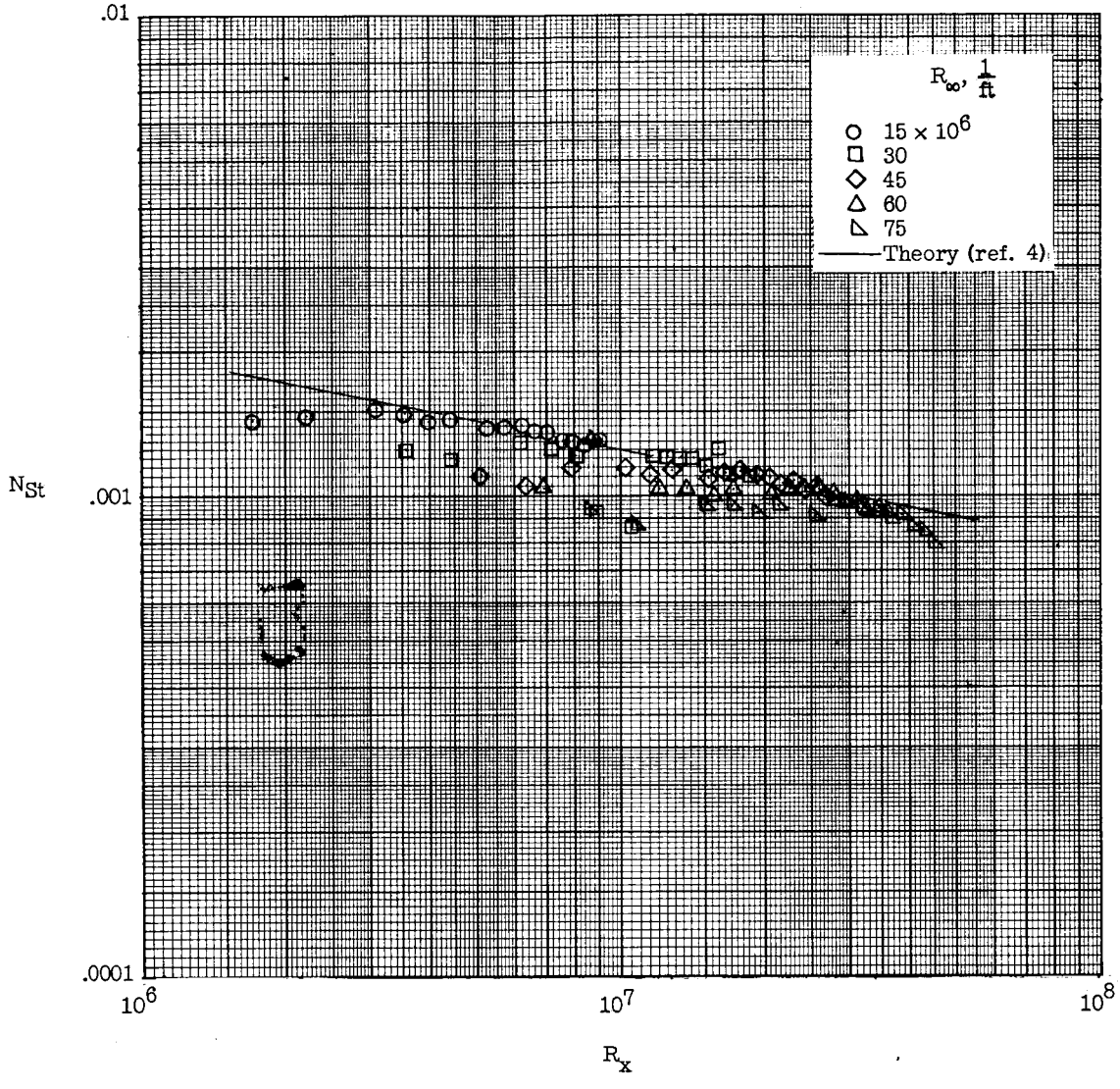

(c) $\alpha = 20^\circ$.

Figure 8.- Concluded.

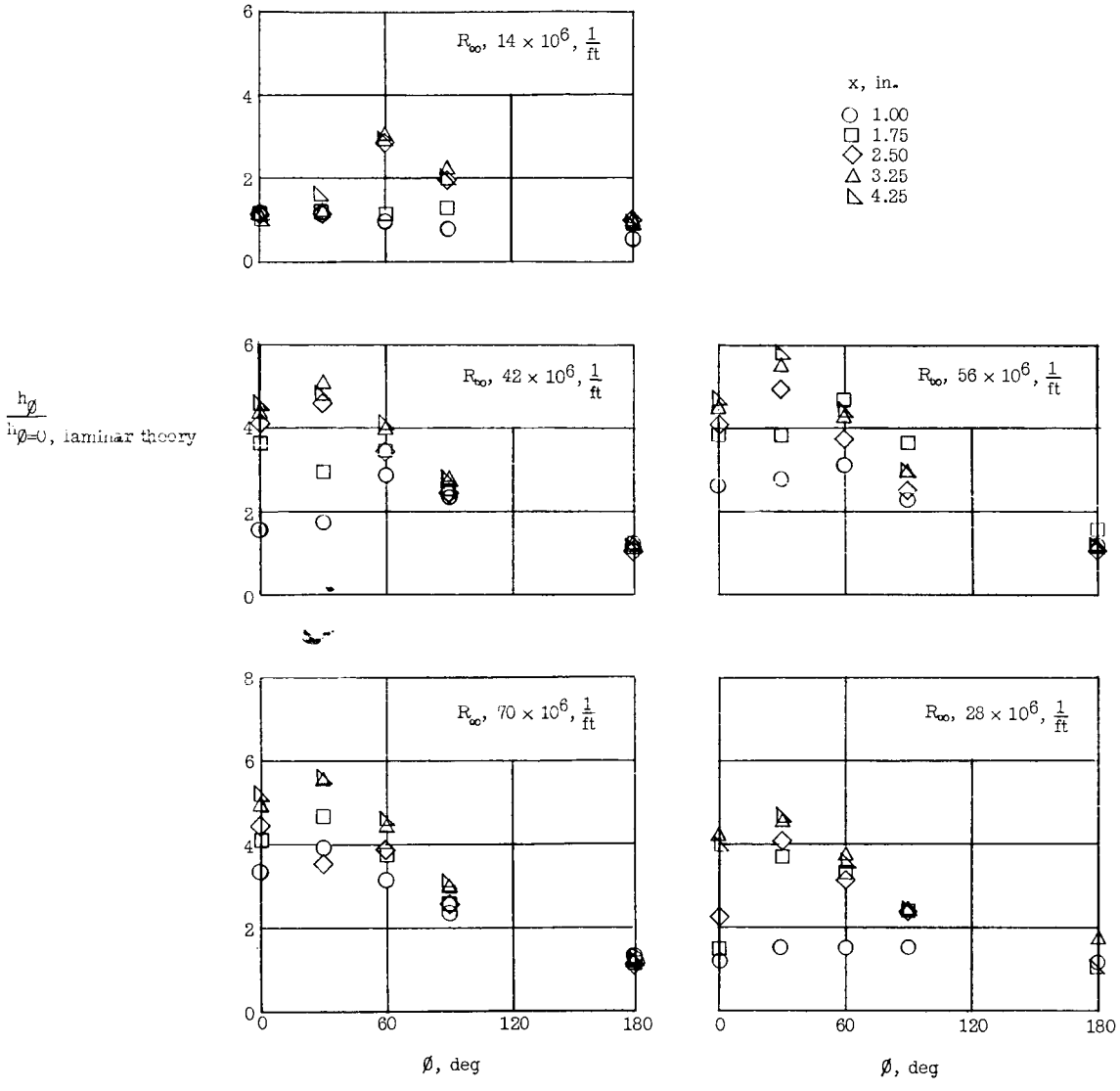

(a) $\alpha = 10^\circ$.

Figure 9.- Peripheral distribution of heat-transfer coefficients.

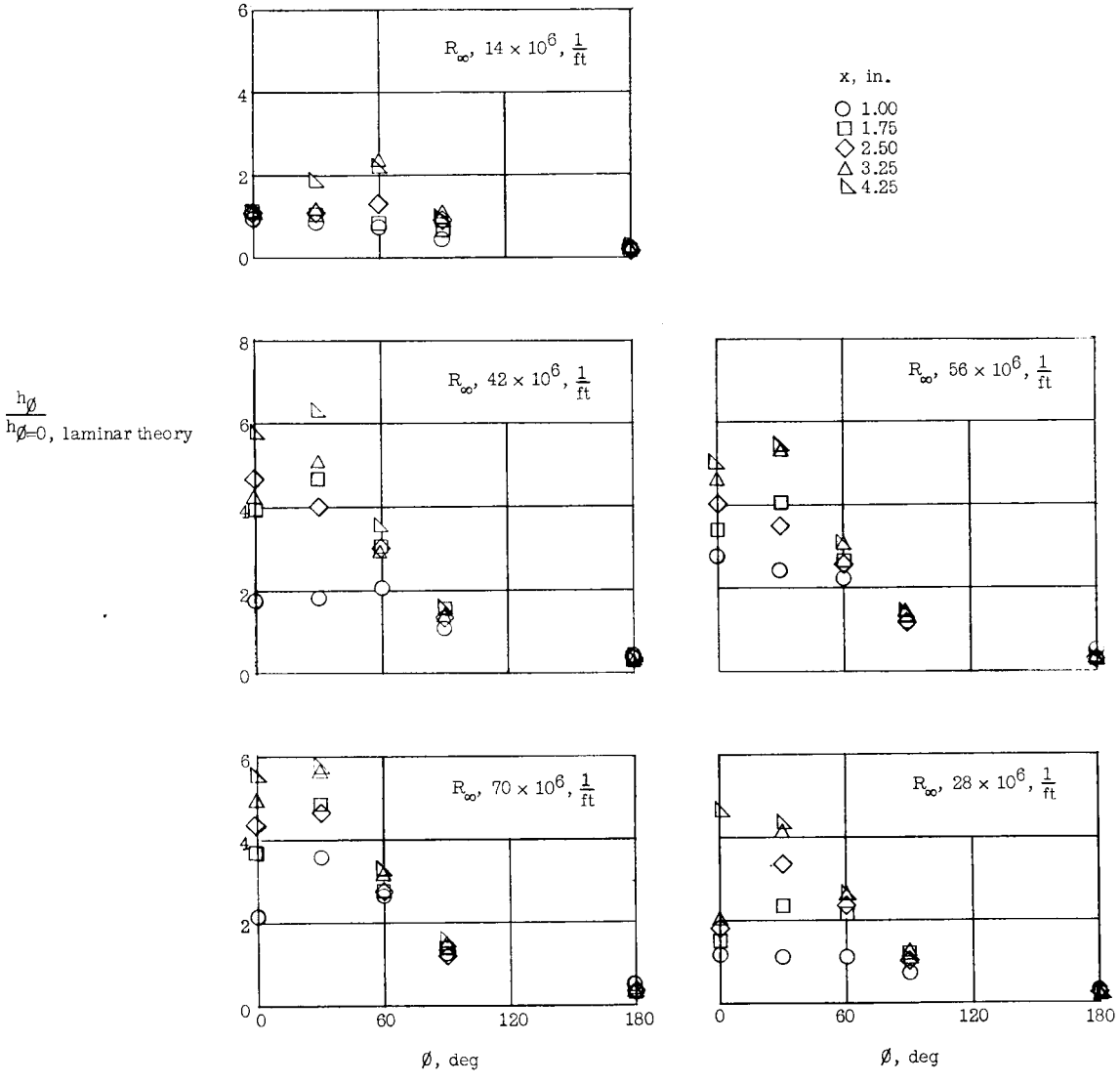

(b) $\alpha = 20^\circ$.

Figure 9.- Concluded.

L-627